Modelling precipitation sequences in power plant steels Part 2 – Application of kinetic theory

J. D. Robson and H. K. D. H. Bhadeshia

New kinetic theory capable of dealing with the simultaneous precipitation of several phases has been applied to a variety of creep resistant power plant steels. It has been demonstrated that the model has the ability to predict the vast differences in precipitation kinetics reported in the published literature for power plant steels. New experimental results on precipitation in a 9Cr1Mo type steel are reported and shown to be consistent with theoretical predictions. *MST/3605*

 Manuscript received 25 April 1996. *The authors are in the Department of Materials Science and Metallurgy, University of Cambridge, Pembroke Street, Cambridge, UK.*

Introduction

The resistance of power plant steels to creep deformation relies greatly on the presence of dispersions of carbides or other particles in the microstructure. These particles not only interfere with the progress of dislocations but also stabilise the microstructure so that features such as lath boundaries change very slowly during long term service at elevated temperatures.

The steels are useful because they take a very long time to reach equilibrium at service temperatures. By implication, the precipitate phases usually present are metastable. Indeed, it is well established that there is usually a sequence of precipitation reactions leading to phases of ever increasing thermodynamic stability. It is very noticeable, during attempts at microstructure calculation, as, for example, in Part 1 of this paper,[1] that there are remarkable differences in the kinetics of precipitation in different steels even when the thermodynamic driving forces are apparently similar.

Experimental studies

Experimental data are required to validate the model. Of particular use are volume fraction *v.* time data for each phase as this enables the model to be verified over the whole range of transformation. More commonly, data are available which indicate the presence or absence of a phase after a particular heat treatment.[2] Such data are also valuable and may be used to check if the onset of precipitation is predicted at the correct time. There have been several studies of the precipitation kinetics in 2·25Cr1Mo type steels (e.g. Ref. 2) that provide suitable data with which to test the model. However, for the 10CrMoV steel, there is a lack of useful data on the evolution of the microstructure from martensite. This is because most experiments have been carried out using as received material which has already undergone a number of severe tempering treatments (e.g. 8 h at 570°C followed by 16 h at 700°C). After such a treatment, carbides which form early in the precipitation sequence (e.g. M_3C) are redissolved while the volume fraction of other carbides is often close to the equilibrium value.

To study the evolution of microstructure in the early stages of tempering, a range of short term heat treatments have been carried out on material in the as quenched condition with the aim of producing a carbide stability diagram for the 10CrMoV steel analogous to those produced for the 2·25Cr1Mo steel.[2] This diagram, along with measurements of the volume fractions after various stages of transformation, has been used to calibrate and test the model.

FURNACE HEAT TREATMENTS

Cylindrical specimens 8 mm in diameter and 12 mm in length were machined from a block of 10CrMoV steel supplied by National Power. The specimens were sealed in silica tubes which were first evacuated and then filled with argon to a pressure of 150 mmHg (20 kPa) to prevent any decarburisation or oxidation. Homogenisation was then carried out for 3 days at 1200°C followed by a rapid (water) quench. The microstructure following this treatment consisted of martensite with a small amount (~0·1%) of δ ferrite. Specimens were then resealed in silica tubes and subjected to a range of heat treatments as given in Table 1.

MICROSCOPY

Carbon replica specimens were prepared from each cylindrical specimen for examination in a Philips 400T transmission electron microscope (TEM). Replicas were prepared following the method of Smith and Nutting.[3] Electrolytic etching in a solution of 5% hydrochloric acid in methanol at 1·5 V was used to remove the carbon film, which was then washed in methylated spirits, floated off in distilled water, and collected on copper grids.

The extraction replicas were then examined in the TEM. Selected area diffraction patterns and dark field micrographs were used to identify and classify the precipitate phases.

Experimental results

The evolution of the microstructure of the 10CrMoV steel during the early stages of tempering is best illustrated by examining the series of micrographs taken from the samples held at 600°C. Figure 1 shows micrographs which are examples of all the transitions observed. Even after only 10 min there were small needles of M_2X precipitated along with M_3C. After 30 min, the M_2X precipitate had intensified while the M_3C volume fraction remained approximately constant. After 1 h there were additional blocky precipitates which were identified as $M_{23}C_6$; M_3C was present as well as M_2X. Finally, after 16 h, the microstructure consisted of relatively large $M_{23}C_6$ particles localised to lath boundaries along with M_2X occurring within the laths. It is also possible that some fine MX phase was present, although none was found in this investigation. The sequence observed may be summarised as follows

$$M_3C + M_2X \rightarrow M_3C + M_2X + M_{23}C_6 \rightarrow M_2X + M_{23}C_6$$

The same sequence was observed at 650°C, although the precipitation kinetics appear to be faster for all phases at

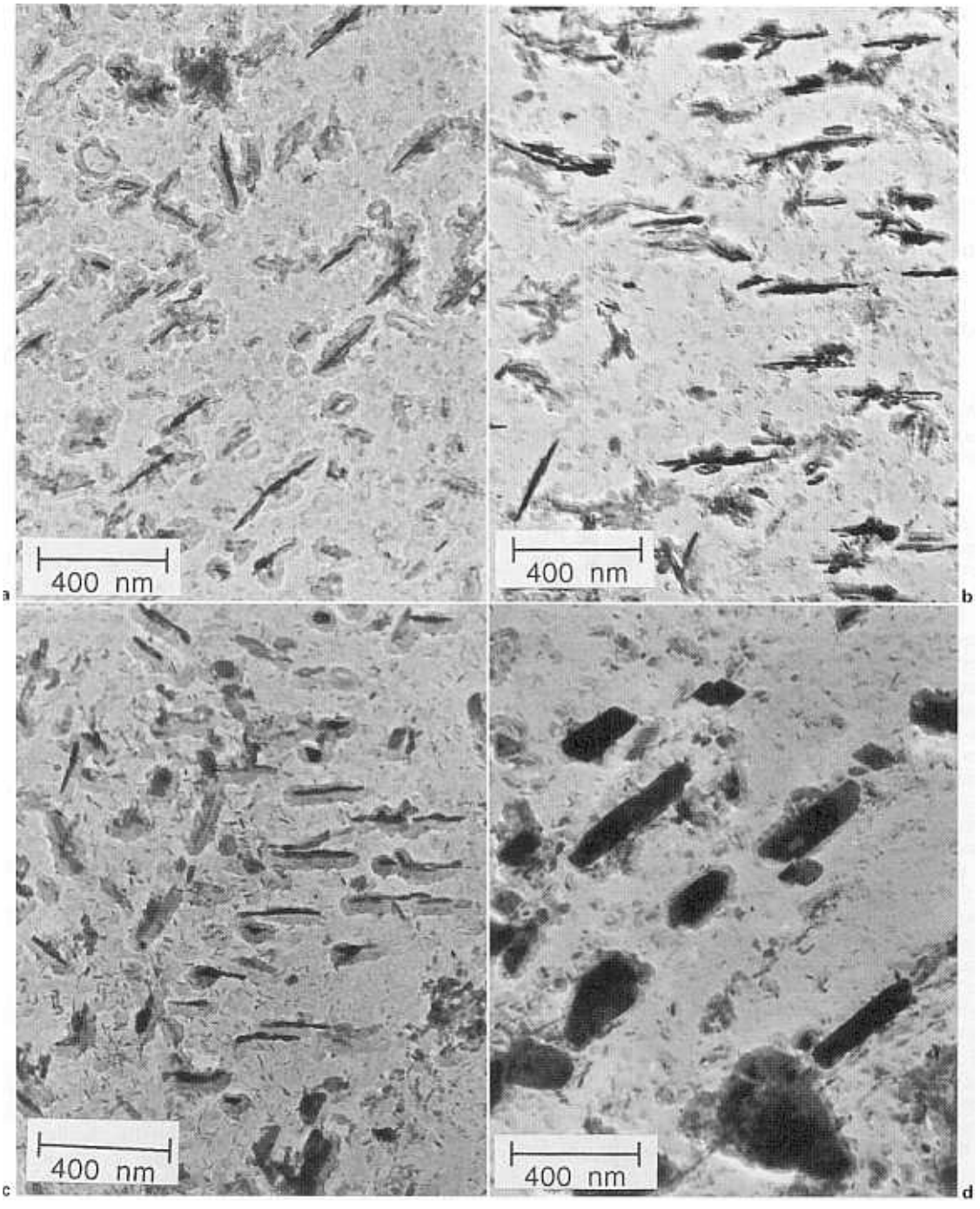

a 10 min; *b* 30 min; *c* 1 h; *d* 16 h

1 Micrographs showing evolution of microstructure in 10CrMoV steel after given times at 600°C

this temperature. At 800°C, $M_{23}C_6$ was observed after only 3 min, by which time M_3C had dissolved (assuming it was present at an earlier time). These results are summarised in an approximate carbide stability diagram (Fig. 2).

Calculated kinetics for M_2X and $M_{23}C_6$

A computer program has been developed which provides volume fraction data as a function of time for a given temperature. Time–temperature–transformation (TTT) diagrams, therefore, can be calculated.

The model was calibrated using three sets of data. Published lengthening rates for molybdenum carbides were successfully compared with calculations. The predicted TTT diagrams were compared with Baker and Nutting's measured carbide stability diagram for the 2·25Cr1Mo steel[2] and with the present authors' measured diagram for the 10CrMoV steel. The aim of the exercise was to produce a single set of model parameters capable of rationalising the vastly different observations for these classic power plant steels.

Table 1 Heat treatments performed on specimens of 10CrMoV steel

Temperature, °C	Time, h
600	0·16, 0·5, 1, 4, 16
650	0·16, 0·5, 2, 8
800	0·05, 0·16

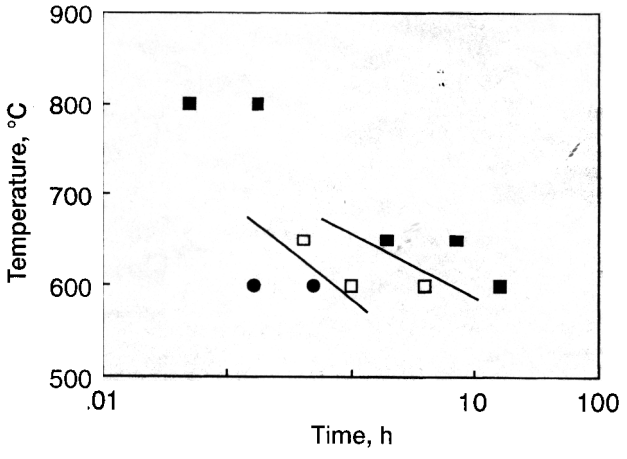

● $M_3C + M_2X$; □ $M_3C + M_2X + M_{23}C_6$; ■ $M_2X + M_{23}C_6$

2 Approximate carbide stability diagram for 10CrMoV steel

The comparisons gave values of the surface energy and site density of nuclei for each phase. The set of these parameters which gave the best fit for the 10CrMoV steel is given in Table 2. It may yet be possible that a different set of these parameters could adequately describe the experimental data. However, it is noteworthy that the interfacial energy correlates with the known position of the phase concerned in the precipitation sequence.

The same parameters were then used to make predictions for the 2·25Cr1Mo steel. Figure 3 shows comparisons between the experimental and predicted TTT diagrams for both steels with lines shown for M_2X and $M_{23}C_6$. The lines plotted in Fig. 3*a* for the 10CrMoV steel correspond to the volume fractions observed for both phases at 600°C. Superimposed on this plot are the corresponding experimental points to enable comparisons to be made.

The original Baker and Nutting data for the 2·25Cr1Mo steel were qualitative;[2] their TTT diagram was plotted with a view to illustrating the point where a phase made its first appearance. To enable a comparison with the present authors' model, it was assumed that a phase became noticeable by TEM when its fraction exceeded 0·01. Calculated curves corresponding to this fraction were plotted for the 2·25Cr1Mo steel alongside Baker and Nutting's observations. Figure 3*b* shows the reasonable agreement obtained. In particular, the model correctly predicts that $M_{23}C_6$ precipitation takes place at much longer times in the 2·25Cr1Mo steel than in the 10CrMoV steel.

Apart from TTT diagrams, the model is able to produce a variety of other types of output. For example, a plot of $(1-\Phi)$ against time for each phase shows how the extent of reaction Φ changes for that phase. At the start of transformation, $(1-\Phi)$ equals 1, and when precipitation is complete, $(1-\Phi)$ equals 0. Figure 4 shows how the extent of reaction varies for both steels at 600°C. The equilibrium precipitates, as predicted by MTDATA, are given in Table 3. At 600°C, the equilibrium precipitate for the 2·25Cr1Mo steel is $M_{23}C_6$, while for the 10CrMoV steel the equilibrium precipitates are $M_{23}C_6$ and M_2X.

Table 2 Values for surface energy and site density for nuclei of each phase which give best fit between prediction and experiment

Phase	Surface energy, J m^{-2}	Site density, m^{-3}
M_2X	0·248	$3·8 \times 10^{16}$
$M_{23}C_6$	0·269	$2·7 \times 10^{15}$
Laves	0·331	$1·1 \times 10^{9}$

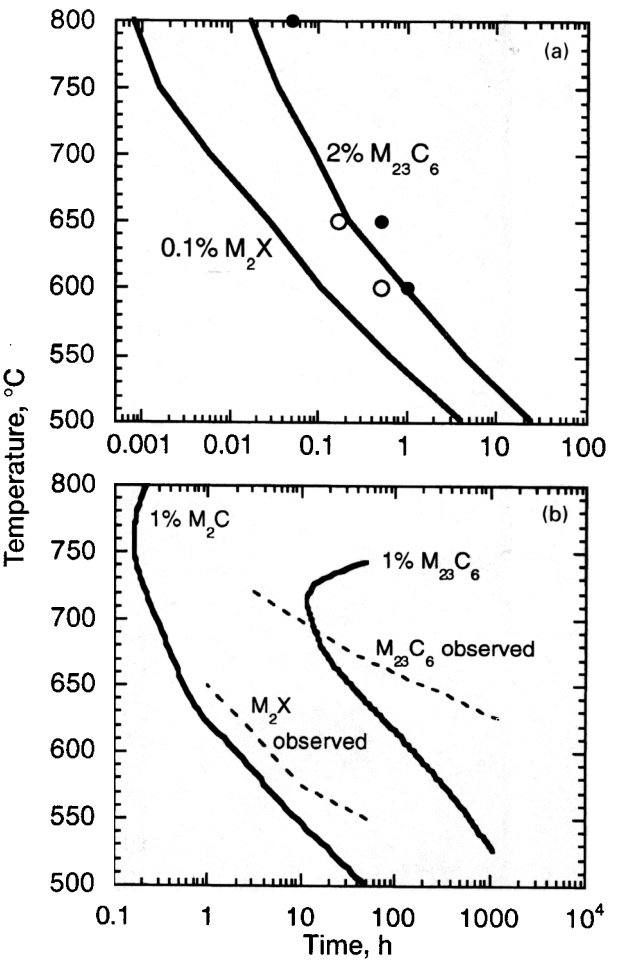

● $M_{23}C_6$ observed; ○ $M_{23}C_6$ not observed
a 10CrMoV, with experimental points made using TEM; *b* 2·25Cr1Mo, with Baker and Nutting's experimental estimates

3 Predicted TTT diagrams for M_2X and $M_{23}C_6$ precipitation in given steels

The intercept of the line for each phase on the horizontal axes of Fig. 4*a* and *b* represents the time when precipitation (or enrichment in the case of M_3C) is complete for that phase. For the 10CrMoV steel, the order of events is as follows (Fig. 4*a*). There is first the rapid completion of M_3C enrichment as the steel has a very large chromium concentration. This is followed by the completion of Laves precipitation; for this particular temperature (600°C), Laves phase is a metastable phase. However, because the precipitation of Laves phase is extremely sluggish, at the time it stops precipitating (~30 min), the volume fraction which has formed is very small ($\sim 2 \times 10^{-9}$). After this time it dissolves rapidly, and so it is in unlikely that it would be experimentally observed. Finally, M_2X and $M_{23}C_6$ form as the equilibrium phases. Note that the extent of reaction for the equilibrium phases is the same at all times, and so the curves for $M_{23}C_6$ and M_2X are identical. Once a metastable phase has completed precipitating (or enriching), it will start to dissolve to provide solute for all

Table 3 Predicted equilibrium precipitate phases for 2·25Cr1Mo steel and 10CrMoV steel

Temperature, °C	2·25Cr1Mo steel	10CrMoV steel
500	$M_{23}C_6$	$M_{23}C_6$, M_2X, Laves
550	$M_{23}C_6$	$M_{23}C_6$, M_2X, Laves
600	$M_{23}C_6$	$M_{23}C_6$, M_2X
650	$M_{23}C_6$	$M_{23}C_6$, M_2X
700	$M_{23}C_6$	$M_{23}C_6$, M_2X

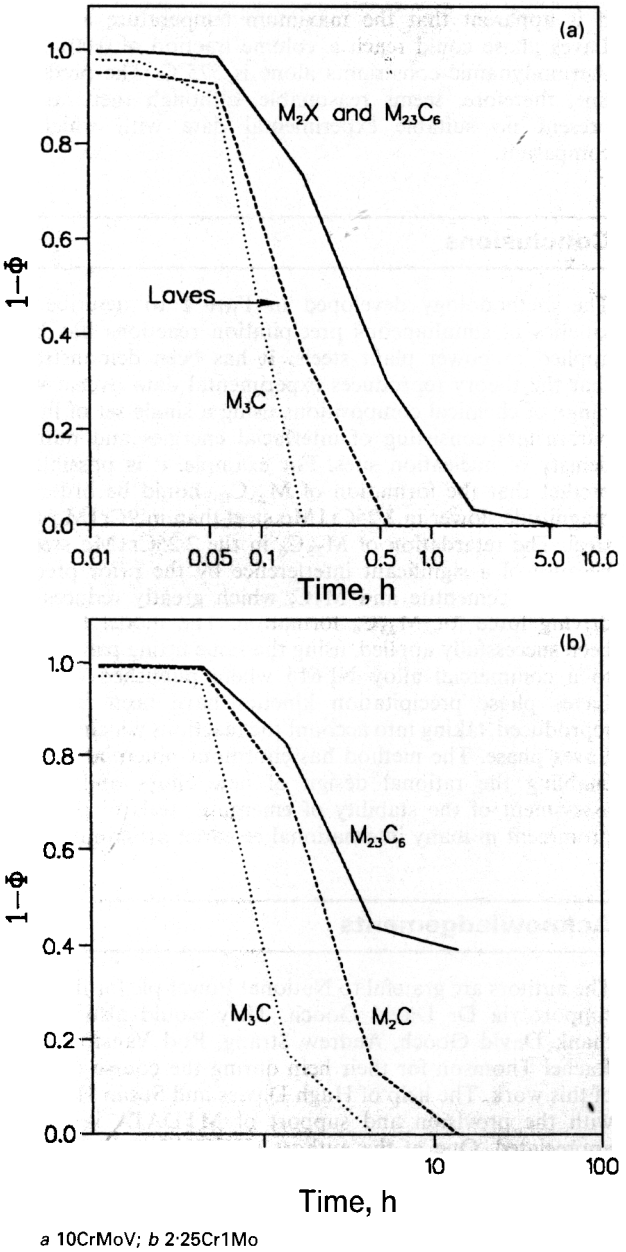

a 10CrMoV; *b* 2·25Cr1Mo

4 Plots showing variation of extent of reaction Φ with time for each phase at 600°C in given steels

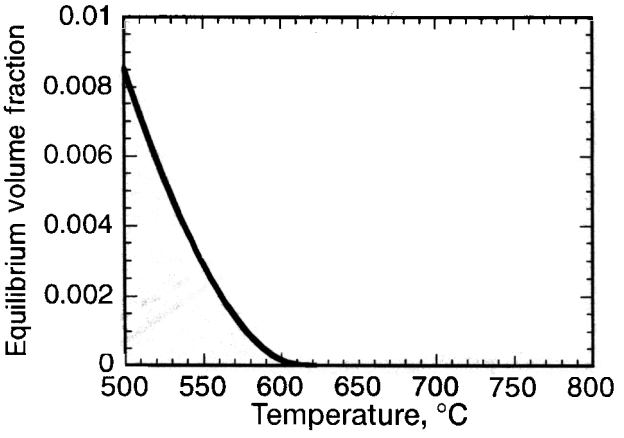

5 Variation of equilibrium volume fraction of Laves phase with temperature in 10CrMoV steel, calculated using MTDATA

the more stable phases whose extent of reaction is less (i.e. $(1-\Phi)$ is greater). So, in the case of the 10CrMoV steel, M_3C and Laves phase eventually dissolve to provide solute to M_2X and $M_{23}C_6$.

In the 2·25Cr1Mo steel (Fig. 4*b*), the order in which precipitation and enrichment events are completed is similar. However, because of the difference in chemical compositions, M_2C precipitation is finished well before $M_{23}C_6$ precipitation, which is not complete within the timescale shown. The reason for this is that the equilibrium volume fractions of M_2C and M_3C are greater in this steel owing to its higher carbon content. Therefore, precipitation or enrichment of these phases removes a greater proportion of the available solute for the matrix than is removed in the 10CrMoV steel. The reduction in the solute available for $M_{23}C_6$ suppresses its formation to later times.

It is interesting that the gradient of the $M_{23}C_6$ line changes when M_3C dissolution starts (Fig. 4*b*). Once M_3C starts dissolving, it does not withdraw solute from the matrix. Furthermore, at this point, M_2C precipitation is almost complete, so that its effect on the matrix solute content becomes extremely small. The change in gradient, therefore, represents the transition from a situation where all three phases are drawing solute to one where only $M_{23}C_6$ is growing. Such a change is less apparent in the 10CrMoV steel (Fig. 4*a*) because the volume fraction of M_3C is considerably smaller and, hence, the proportion of solute it claims from the matrix is also relatively small. It must be noted that in this model the precipitation of M_7C_3 has been ignored. This phase was observed by Baker and Nutting[2] after the formation of M_2C but before $M_{23}C_6$. Accounting for this phase would further suppress $M_{23}C_6$ formation as there would be increased competition for the solute in the matrix, and may lead to better agreement between the predicted and experimental TTT curves.

Calculated kinetics for Laves phase

Laves phase is an equilibrium precipitate at temperatures below ~600°C in the 10CrMoV steel. The variation of the equilibrium volume fraction with temperature is shown in Fig. 5. This is consistent with experimental work which shows that Laves phase is observed after 30 000 h at 600°C but not at 650°C.[4]

Currently, the number of data points available for Laves phase precipitation in this steel are insufficient to enable calibration of the model for this phase. However, the model is not restricted in its application to any particular class of steels. There are data in the literature on the precipitation of Laves phase in the 9CrMoWV steel NF616, a commercial alloy designated for service at temperatures in excess of 600°C in power plant.[5] The steel (wt-%: Fe–0·106C–8·96Cr–0·47Mo–0·051N–0·069Nb–0·20V–1·83W) contains tungsten which makes it more susceptible to Laves formation, which occurs over a greater range of temperatures than in the 10CrMoV steel.

There have been a number of studies of Laves phase precipitation in NF616 (Refs. 5 and 6) that provide suitable data with which to test the model. Hald[6] has developed a model for the precipitation of Laves phase; the model begins with an assumed number density of particles which then grow at a diffusion controlled rate. After fitting at a particular temperature, the model was successfully applied to predict the fraction of Laves phase as a function of temperature and time, taking into account changes in the equilibrium compositions and diffusivity with temperature. Figure 6*a* shows a comparison between the TTT curve estimated using the simultaneous kinetics model and the results of Hald's model for the same volume fraction, for

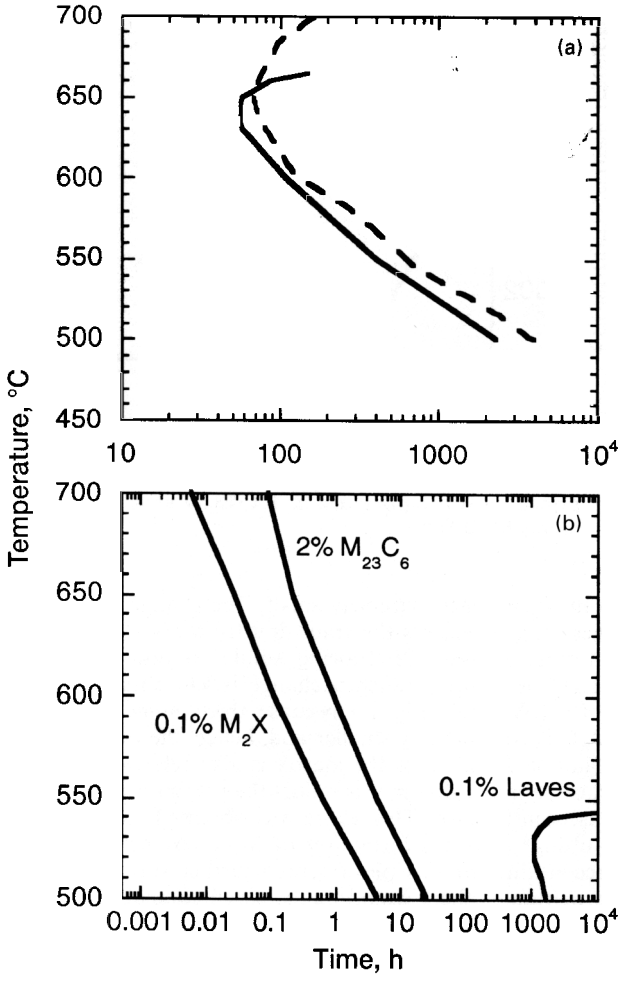

a 9CrMoWV, —— 0·25% predicted and - - - - 0·25% calculated by Hald; *b* 10CrMoV, 0·1% with lines for M_2X and $M_{23}C_6$

6 Predicted TTT diagrams for Laves phase precipitation in given steels

NF616. The lines for M_2X and $M_{23}C_6$ which are also predicted using the simultaneous model have been omitted from the diagram for clarity. The agreement between the model of the present authors and that of Hald is reasonable. The values for the surface energy and number of sites for Laves phase nucleation are given in Table 2, together with the values used for M_2X and $M_{23}C_6$ which are the same for all the steels of the present investigation.

The simultaneous kinetics model was then used to predict the precipitation kinetics of Laves phase in the 10CrMoV steel using the same values for nucleation site density and surface energy (as given in Table 2). Figure 6*b* shows the complete TTT diagram for this steel, including a line plotted for Laves phase corresponding to a volume fraction of 0·001. This shows that Laves phase is predicted to reach this volume fraction after ~1000 h up to 550°C. Above ~560°C, the time taken for Laves phase to reach this volume fraction tends towards infinity. Referring to Fig. 5, it is apparent that the maximum temperature at which Laves phase could reach a volume fraction of 0·001 from thermodynamic constraints alone is 575°C. The predicted line, therefore, seems reasonable, although there are at present no suitable experimental data with which to compare it.

Conclusions

The methodology developed in Part 1 to describe the kinetics of simultaneous precipitation reactions has been applied to power plant steels. It has been demonstrated that the theory reproduces experimental data over a wide range of chemical compositions using a single set of fitting parameters consisting of interfacial energies and number density of nucleation sites. For example, it is possible to predict that the formation of $M_{23}C_6$ should be orders of magnitude slower in 2·25Cr1Mo steel than in 9Cr1Mo type steel. The retardation of $M_{23}C_6$ in the 2·25Cr1Mo steel is because of a significant interference by the prior precipitation of cementite and M_2C, which greatly reduces the driving force for $M_{23}C_6$ formation. The model has also been successfully applied, using the same fitting parameters, to a commercial alloy NF616 where published data on Laves phase precipitation kinetics have been faithfully reproduced, taking into account the reactions which precede Laves phase. The method has enormous potential both in enabling the rational design of new alloys and in the assessment of the stability of emerging steels of the kind prominent in many international research programmes.

Acknowledgements

The authors are grateful to National Power plc for financial support via Dr David Gooch. They would also like to thank David Gooch, Andrew Strang, Rod Vanstone, and Rachel Thomson for their help during the course of some of this work. The help of Hugh Davies and Susan Hodgson with the provision and support of MTDATA is greatly appreciated. One of the authors (HKDHB) is grateful to the Royal Society for a Leverhulme Trust Senior Research Fellowship.

References

1. J. D. ROBSON and H. K. D. H. BHADESHIA: *Mater. Sci. Technol.*, 1997, **13**, 631–639.
2. R. G. BAKER and J. NUTTING: *J. Iron Steel Inst.*, 1959, **192**, 257–268.
3. R. SMITH and J. NUTTING: *J. Iron Steel Inst.*, 1959, **192**, 314–329.
4. R. W. VANSTONE: in Proc. Conf. 'Materials for advanced power engineering', Liège, Belgium, October 1994, Centre de Recherche Métallurgique.
5. M. OHGAMI, H. MIMURA, H. NAOI, and T. FUJITA: in Proc. 5th Int. Conf. on 'Creep of Materials', Lake Buena Vista, FL, USA, May 1992, ASM International.
6. H. MIMURA, M. OHGAMI, H. NAOI, and J. HALD: *Zairyo to Purosesca (CAMP–ISIJ)*, 1994, **7**, 809.